Carrier-envelope phase locking of multi-pulse lasers with an intra-cavity Mach-Zehnder interferometer

Mark Shtaif,[1,*] Curtis R. Menyuk,[2] Michael L. Dennis,[3] and Michael C. Gross[3]

[1] *School of Electrical Engineering, Faculty of Engineering, Tel Aviv University, Tel Aviv, 69978, Israel*

[2] *Computer Science and Electrical Engineering Department, University of Maryland Baltimore County, 1000 Hilltop Circle, Baltimore, MD 21250, USA*

[3] *Air and Missile Defense Department, Johns Hopkins University Applied Physics Laboratory, 11100 Johns Hopkins Rd, Laurel, MD, USA*

[*] *shtaif@eng.tau.ac.il*

Abstract: We propose the use of an intra-cavity Mach Zehnder interferometer (MZI), for increasing the repetition rate at which carrier-envelope phase-locked pulses are generated in passively mode-locked fiber lasers. The attractive feature of the proposed scheme is that light escaping through the open output ports of the MZI can be used as a monitor signal feeding a servo loop that allows multiple pulses to co-exist in the cavity, while rigidly controlling their separation. The proposed scheme enables in principle a significant increase in the pulse-rate with no deterioration in the properties of the generated pulses.

OCIS codes: (140.3510) Fiber lasers; (140.4050) Mode-locked lasers.

References and links

1. D. J. Jones, S. A. Diddams, J. K. Ranka, A. Stentz, R. S. Windeler, J. L. Hall, and S. T. Cundiff, "Carrier-envelope phase control of femtosecond mode-locked lasers and direct optical frequency synthesis," Science **288**, 635–639 (2000).
2. R. Holzwarth, Th. Udem, T. W. Hänsch, J. C. Knight, W. J. Wadsworth, and P. St. J. Russell, "Optical frequency synthesizer for precision spectroscopy," Phys. Rev. Lett., **85**, 2264–2267 (2000).
3. I. Coddington, W. C. Swann, and N. R. Newbury, "Coherent multiheterodyne spectroscopy using stabilized optical frequency combs," Phys. Rev. Lett. **100**, 013902 (2008)
4. S. M. Foreman, K. W. Holman, D. D. Hudson, D. J. Jones, and J. Ye, "Remote transfer of ultrastable frequency references via fiber networks," Rev. Sci. Instrum. **78**, 021101 (2007).
5. S. A. Diddams, J. C. Bergquist, S. R. Jefferts, and C. W. Oates, "Standards of time and frequency at the outset of the 21st century," Science **306**, 1318–1324 (2004).
6. J. J. McFerran, E. N. Ivanov, A. Bartels, G. Wilpers, C. W. Oates, S. A. Diddams, and L. Hollberg, "Low-noise synthesis of microwave signals from an optical source," Electron. Lett. **41**, 650–651 (2005).
7. S. A. Diddams, " The evolving optical frequency comb," J. Opt. Soc. Am. B. **27**, B51–B62 (2010).
8. A. Bartels, D. Heinecke, and S. A. Diddams, "10-GHz self-referenced optical frequency comb," Science, vol. 326, p. 681 (2009).
9. D. A. Howe and A. Hati, "Low-noise X-band oscillator and amplifier technologies: Comparison and status," Proc. 2005 Int. Freq. Control Symp. and Precise Time and Time Interval Sys. Mtg. IEEE: Piscataway, NJ, 2005, 481–487.
10. I. Hartl, A. Romann, and M. E. Fermann, "Passively mode locked GHz femtosecond Yb-fiber laser using an intra-cavity martinez compressor," Proc. Conf. Lasers and Electro-Optics 2011, Optical Society of America, paper CMD3.

#150450 - $15.00 USD Received 5 Jul 2011; revised 26 Aug 2011; accepted 8 Sep 2011; published 1 Nov 2011

11. J. Chen, J. W. Sickler, P. Fendel, E. P. Ippen, F. X. Kärtner, T. Wilken, R. Holzwarth, and T. W. Hänsch, "Generation of low-timing-jitter femtosecond pulse trains with 2 GHz repetition rate via external rate multiplication," Opt. Lett. **33**, 959–961 (2008).
12. S. A. Diddams, M. Kirchner, T. Fortier, D. Braje, A. M. Weiner, and L. Hollberg, "Improved signal-to-noise ratio of 10 GHz microwave signals generated with a mode-filtered femtosecond laser frequency comb," Opt. Express **17**, 3331–3340 (2009).
13. N. R. Newbury and W. C. Swann, "Low-noise fiber-laser frequency combs," J. Opt. Soc. Am. B **24**, 1756–1770 (2007).
14. J. W. Dawson, M. J. Messerly, R. J. Beach, M. Y. Shverdin, E. A. Stappaerts, A. K. Sridharan, P. H. Pax, J. E. Heebner, C. W. Siders, and C. P. J. Barty, "Analysis of the scalability of diffraction-limited lasers and amplifiers to high average power," Opt. Express **16**, 13240–13266 (2008).
15. T. R. Schibli, I. Hartl, D. C. Yost, M. J. Martin, M. Marcinkevičius, M. E. Fermann, and J. Ye, "Optical frequency comb with submillihertz linewidth and more than 10 W average power," Nature Photon. **2**, 355–359 (2008).
16. E. Yoshida, Y. Kimura, M. Nakazawa, "Laser diode-pumped femtosecond Erbium doped fiber laser with a subring cavity for repitition rate control," Appl. Phys. Lett. **60**, 932–934 (1992).
17. G.T. Harvey and L.F. Mollenauer, "Harmonically mode-locked fiber ring laser with an internal Fabry-Perot stabilizer for soliton transmission," Opt. Lett. **18**, 107–109 (1993).
18. O. Pottiez, O. Deparis, R. Kiyan, M. Haelterman, P. Emplit, P. Mégret, and M. Blondel, "Supermode noise of harmonically mode-locked erbium fiber lasers with composite cavity," IEEE J. Quantum Electron., **38**, 252–259 (2002).
19. Y. Parkhomenko, M. Horowitz, C. R. Menyuk, and T. F. Carruthers, "Theoretical study of an actively modelocked fiber laser stabilized by an intra-cavity Fabry-Perot etalon: Linear regime," J. Opt. Soc. Am. B. **24**, 1793–1802 (2007).
20. F. Quinlan, S. Ozharar, S. Gee, and P. J. Delfyett, "Harmonically modelocked semiconductor-based lasers as high repetition rate ultralow noise pulse train and optical frequency comb sources," J. Opt. A: Pure Appl. Opt. **11**, 1–23 (2009)
21. R. P. Davey, N. Langford, and A. I. Ferguson, "Interacting solitons in erbium fibre laser," Electron. Lett. **27**, 1257–1258 (1991).
22. J. Schröder, S. Coen, F. Vanholsbeeck, and T. Sylvestre, "Passively modelocked fiber Raman laser with 100 GHz repetition rate," Opt. Lett. **31**, 3489–3491 (2006).
23. D. Panasenko, P. Polynkin, A. Polynkin, J. V. Moloney, M. Mansuripur, and N. Peyghambarian, "Er-Yb femtosecond ring fiber oscillator with 1.1-W average power and GHz repetition rates," IEEE Photon. Technol. Lett. **18**, 853–855 (2006).
24. A. N. Pilipetskii, E. A. Golovchenko, and C. R. Menyuk, "Acoustic effect in passively mode-locked fiber ring lasers," Opt. Lett. **20**, 907–909 (1996).
25. B. R. Washburn, S. A. Diddams, N. R. Newbury, J. W. Nicholson, M. F. Yan, and C. G. Jørgenson, "Phase-locked, erbium-fiber-laser based frequency comb in the near infrared," Opt. Lett., vol. 29, 250–252 (2004).
26. P. Pal, W. H. Knox, I. Hartl, and M. E. Fermann, "Self referenced Yb-fiber-laser frequency comb using a dispersion micromanaged tapered holey fiber," Opt. Express **15**, 12161–12166 (2007).
27. E. Baumann, F. R. Giorgetta, J. W. Nicholson, W. C. Swann, I. Coddington, and N. R. Newbury, "High-performance, vibration-immune, fiber-laser comb, Opt. Lett., **34**, 638–640 (2009).
28. J. Lim, K. Knabe, K. A. Tillman, W. Neely, Y. Wang, R. Amezcua-Correa, F. Couny, P. S. Light, F. Benabid, J. C. Knight, K. L. Corwin, J. W. Nicholson, and B. R. Washburn, "A phase-stabilized nanotube fiber laser frequency comb," Opt. Express **17**, 14115–14120 (2009).
29. S. K. Sheem, "Optical fiber interferometers with $[3 \times 3]$ directional couplers: Analysis," J. Ap. Phys. **52**, 3865–3872 (1981).
30. R. W. C. Vance and J. D. Love, "Design procedures for passive planar coupled waveguide devices," IEE Proc. Opto-Electron. **141**, 231–241 (1994).
31. At the time of this writing, companies that produce 3×3 fiber couplers include the Shenzhen Technology Company and Rayscience Optoelectronic Innovation.
32. R. G. Priest, "Analysis of fiber interferometer utilizing 3×3 fiber coupler," Trans. Micro. Theory Tech. **MTT-30**, 1589–1591 (1982).
33. H. A. Haus, J . G. Fujimoto, and E. P. Ippen, "Structures for additive pulse mode locking, J. Opt. Soc. Amer. E, **8**, 2068–2076 (1991).
34. C. Antonelli, J. Chen and F. Kartner, "Intracavity pulse dynamics and stability for passively mode-locked lasers," Opt. Express **15**, 5919–5924 (2007).
35. H. A. Haus, A.Mecozzi, "Noise of mode-locked lasers," IEEE J. Quantum Electron. **29**, 983–995 (1993).
36. F. M. Gardner, *Phaselock techniques* 3rd ed. (Wiley-Interscience, 2005).
37. S. T. Cundiff, J. Ye, and J. L. Hall, "Optical Frequency Synthesis Based on Mode-Locked Lasers," Review of Scientific Instruments, **72**, 3749–3771, (2001).

#150450 - $15.00 USD Received 5 Jul 2011; revised 26 Aug 2011; accepted 8 Sep 2011; published 1 Nov 2011

1. Introduction

The invention of carrier-envelope-phase locking (CEPL) of passively modelocked lasers a decade ago [1, 2] has revolutionized the measurement of frequencies and has important potential applications to chemical sensing [3], time transfer [4], time-keeping [5], and microwave generation [6]. In the last five years, a wide variety of passively modelocked lasers have been phase-locked using CEPL [7]. CEPL works by stabilizing both the repetition rate of the laser and the carrier-envelope phase offset (pulse-to-pulse phase change) using two electronic feedback loops, so that a stabilized frequency comb that acts like a frequency ruler is produced. CEPL lasers operate in a frequency range of 100–300 THz and typical repetition rates are below 2 GHz in solid-state lasers and below 500 MHz in fiber lasers. For many applications, it would be advantageous to have a frequency spacing between comb lines that is on the order of 10 GHz or more. In particular, it has been demonstrated that the phase noise from the 10 GHz tones of the electronic signal that emerges from a photodetector can be as much as 25 dB below the best dielectric resonant RF oscillators at 100 Hz from the carrier [8], and these tones could be produced more efficiently from a laser whose basic repetition rate was 10 GHz. However, this frequency spacing is difficult to achieve with passively modelocked lasers. The comb spacing equals the repetition rate, which is inversely proportional to the laser's length, and it is not easy to achieve sufficient gain in a cavity of this size for CEPL, although it has recently been done for a Ti:sapphire laser [9]. In an ytterbium-doped fiber laser, a repetition rate of 1.3 GHz was recently demonstrated [10], but this laser has many bulk components, and the repetition rate of fiber lasers is typically below 500 MHz. It is possible to multiply the repetition rate of a CEPL laser by using an external Fabry-Perot cavity [11, 12], but this approach has the drawback that it divides down the individual pulse energies.

An attractive alternative — particularly for fiber lasers — is to create a CEPL laser with multiple pulses in the laser cavity, spaced a constant time interval apart and with a constant pulse-to-pulse offset. Since the pulse energy is determined by the balance between nonlinearity and dispersion, multiplying the number of pulses does not in theory diminish the pulse energy, although it does require a proportional increase in the average power in the laser cavity and thus the pump power. Since an average power less than 10 mW is sufficient for CEPL locking of lasers [13], while fiber lasers can support average powers in excess of 1 kW [14] and CEPL lasers with an average power of 10 W have been reported [15], a multiplication factor of N greater than 100 is in principle available. Moreover, since the number of comb lines is divided by N, the power in each comb line is multiplied by N^2 — an attractive scaling.

Multi-pulse fiber lasers are not new. Actively modelocked, multi-pulse lasers have long been available. Moreover, it has long been possible to lock the repetition rates [16–19], although these lasers are often troubled by 2π phase slips that lead to hopping between supermodes. Supermodes can be strongly suppressed in this configuration by the use of Fabry-Perot etalons, but cannot be completely eliminated [20]. Multi-pulse passively modelocked lasers are also available [21–23]. While it is possible in some parameter regimes to lock the repetition rate of these lasers by making use of the acoustic effect [23, 24], this locking is fragile in practice, limiting the usefulness of these lasers.

Here, we describe an approach that uses an intra-cavity Mach-Zehnder interferometer (MZI) to couple neighboring pulses in a CEPL laser. While the optical portion of our scheme is similar to schemes that were introduced in actively modelocked lasers [16–19], our implementation introduces a third electronic feedback loop and a simple, intrinsic monitor signal that allows continuous control of the MZI's setting, which is imperative to maintain CEPL operation. Because the number, spacing and phase relation of the pulses is rigidly controlled in this scheme, pulse dropouts are not possible and supermodes are suppressed. We discuss the effectiveness of the proposed feedback mechanism and describe the effect of imperfectly matched MZI param-

#150450 - $15.00 USD Received 5 Jul 2011; revised 26 Aug 2011; accepted 8 Sep 2011; published 1 Nov 2011

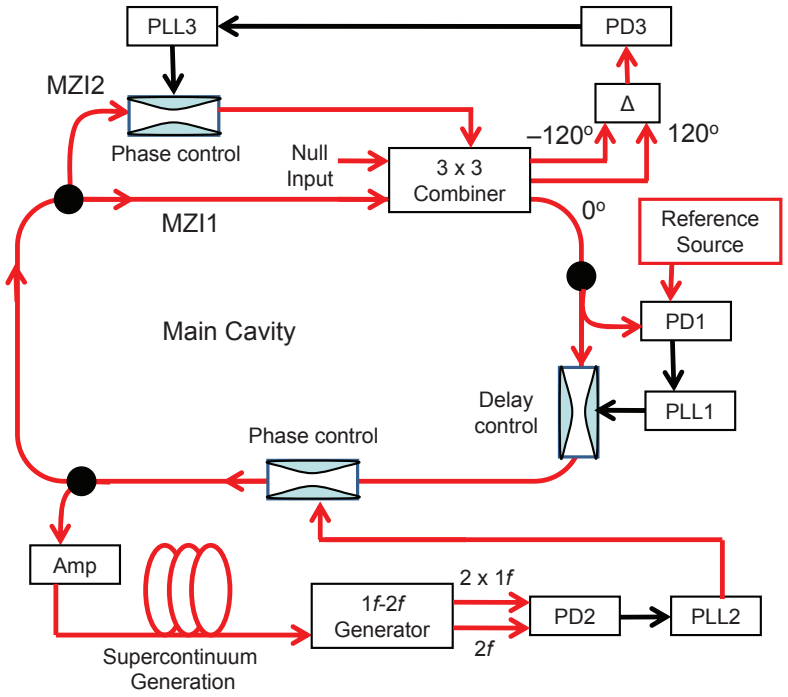

Fig. 1. Schematic illustration of the proposed multi-pulse carrier-envelope phase-locked laser.

eters on the properties of the generated pulses.

2. The MZI enhanced laser set-up

The laser setup that we are considering is shown schematically in Fig. 1 and includes an MZI in a ring laser cavity. In this scheme, we are proposing the use of three feedback loops. The first two are conventional and control the time and phase delays in the main cavity. The third is novel in the context of CEPL lasers and controls the phase difference between the two arms of the Mach-Zehnder interferometer. It plays a role that is analogous to the Fabry-Perot etalon in some harmonically modelocked lasers [20]. In Fig. 1, we focus on the electronic control elements, rather than the optical elements in the main cavity. CEPL has been demonstrated with fiber lasers in which the gain elements are erbium [25] and ytterbium [26]. A variety of fast saturable absorbers have been used, including nonlinear polarization rotation [25], Sagnac loops [27], nanotubes [28], and semiconductor absorbers [26]. There is no reason to doubt that CEPL can used with any passively modelocked laser that produces sufficient power once the two electronic feedback loops that control the time and phase delays in the main cavity have been added. Similarly, the scheme that we are proposing should work with any CEPL laser with sufficient power, once the MZI and the third electronic feedback loop has been added. Indeed, this approach should work with Ti:sapphire lasers, just as well as with fiber lasers. However, the motivation to use this technique with Ti:sapphire lasers is lower than in the case of fiber lasers, because repetition rates as high as 10 GHz can be directly obtained [9].

The first feedback loop controls the length of the main cavity. A reference source is locked to a comb line using heterodyne detection in a photodetector (PD1). The error signal is fed into a phase-locked loop (PLL1), which then controls the delay time, typically using a fiber stretcher.

#150450 - $15.00 USD Received 5 Jul 2011; revised 26 Aug 2011; accepted 8 Sep 2011; published 1 Nov 2011

The second feedback loop controls the difference between the phase and group velocities and hence the carrier-envelope offset frequency. The output signal from the laser is amplified and its bandwidth is increased using supercontinuum generation. Second harmonic generation is then used to double the frequency of a low-frequency comb line in the $1f$–$2f$ generator. This signal is then compared to a comb line at a frequency that approximately equals $2f$, using heterodyne detection in a photodetector (PD2). The error signal is fed into a phase-locked loop (PLL2), which then controls the offset frequency by controlling the roundtrip phase in the main cavity. Typically phase control is realized by controlling the gain and hence the amplitude of the modelocked pulses. The third feedback loop, described in more detail in what follows, controls the phase delay in one arm of the intra-cavity MZI (MZI2) relative to the other arm (MZI1). The time delay in MZI2 is longer than the time delay in MZI1 by approximately T_R/N and the phase difference between MZI2 and MZI1 is approximately θ_R/N, where N is the number of pulses in the laser cavity, whereas the terms T_R and θ_R are the main cavity roundtrip time and phase, respectively. The signals in the two arms of the interferometer are combined, along with a null signal, in a 3×3 combiner, which produces a combined output at differences of 0°, 120°, and -120°. The output at 0° contains most of the input power, so that only a small fraction of the power is lost in the device. The outputs at 120° and -120° are differenced in an interferometer (Δ), and the output is used to create the error signal in a photodetector (PD3). This error signal will be zero when the signals in MZI1 and MZI2 are in phase, and its derivative will be maximum. This error signal is fed into a phase-locked loop (PLL3), which then controls the phase in MZI2. A fiber squeezer can be exploited for controlling the phase in MZI2, and, since the index difference between the two arms of the interferometer is small, one can obtain interferometric control over the phase difference with a macroscopic change in the fiber squeezer.

While 3×3 couplers and their operation are less well-known than 2×2 couplers, they have been demonstrated in a fused-fiber configuration in 1981 [29] and in a bulk waveguide configuration in 1994 [30]. They are available commercially [31]. We briefly summarize their key features for our application, assuming that there are no nonlinear interactions in the device. The 3×3 coupler consists of three identical waveguides that are brought into close proximity, so that their fields couple. The two MZI inputs go into the waveguides that we denote 1 and 3, and the null input goes into waveguide 2. The output labeled 0° in Fig. 1 corresponds to the output of waveguide 2, and the other outputs correspond to waveguides 1 and 3. Assuming that waveguides 1 and 3 couple symmetrically to waveguide 2 — which is necessary for our application — the evolution of the mode amplitudes is given by [29]

$$\frac{dA_1}{dz} = iaA_2 + ibA_3, \quad \frac{dA_2}{dz} = iaA_1 + iaA_3, \quad \frac{dA_3}{dz} = ibA_1 + iaA_3, \tag{1}$$

where A_1, A_2, and A_3 denote the mode amplitudes, while a and b denote the coupling coefficients. The description of the 3×3 coupler in the last paragraph corresponds to the completely symmetric coupler in which $a=b$ [32]. However, this identity is not necessary for the device to work. Writing the phase offset of the two ports in the Mach-Zehnder interferometer as $\Delta\theta_M$ and the amplitude that enters each of the ports as α, we find that the amplitudes at the output may always be written to within an arbitrary phase as $A_1 = C_1\alpha\cos\Delta\theta_M - i\alpha\sin\Delta\theta_M$, $A_2 = C_2\alpha\cos\Delta\theta_M$, and $A_3 = C_1\alpha\cos\Delta\theta_M + i\alpha\sin\Delta\theta_M$, where C_1 and C_2 are complex constants that depend on a and b and on the propagation distance through the coupler. The point to note is that regardless of the values of A and B, the difference $\Delta = A_1 - A_3$ is always proportional to $\sin\Delta\theta_M$, so that the result is insensitive to the propagation length through the coupler and the values of a and b. In the case of a completely symmetric guide at the optimal coupling length, we obtain $C_1 = \alpha/3$ and $C_2 = 4\alpha/3$, so that $8/9$ of the original power is delivered at the output of waveguide 2. The other $1/9$ of the original power is lost by the differencing. In principle,

#150450 - $15.00 USD Received 5 Jul 2011; revised 26 Aug 2011; accepted 8 Sep 2011; published 1 Nov 2011

one can further reduce the power that is lost when differencing by using configurations in which $b < a$.

The differential time and phase delays in the MZI are denoted by T_M and θ_M, respectively. When the MZI parameters are set such that T_R/T_M and θ_R/θ_M are identical and exactly equal to an integer value N, then a pulse train at a repetition period of T_M is an equilibrium solution for the MZI-enhanced mode-locked laser, implying that the repetition rate is larger by a factor of N than when no MZI is present. Provided that the cavity gain is enhanced in order to compensate for the increased average power and for the insertion loss of the MZI, and assuming that T_M is larger than the pulse duration by at least a factor of ten, so that there is no interaction between the pulses — a condition that is easily achievable in practice — the individual pulses in the pulse train are exactly identical to the pulses that would be formed in the same laser in the absence of the MZI. The physics behind this steady-state solution is not hard to understand. Given these perfect conditions in which $T_R = NT_M$ and $\theta_R = N\theta_M$, the spectral comb lines of the field in the cavity coincide exactly with the transmission peaks of the MZI, so that the MZI has no effect on the individual pulse waveforms.

On the other hand, when the differential phase and time delay of the MZI are slightly offset from their optimal values, the MZI interferes with normal pulse generation such that the waveform of the generated pulses, as well as the inter-pulse delay and phase-slip are affected by its presence. If the MZI parameters are allowed to wander farther from their ideal values, the laser will eventually lose its ability to generate pulses and will switch to continuous wave operation. It is the role of the MZI servo loop to prevent this breakdown from occurring. This loop continuously controls the phase delay between the MZI arms so that it stays closely matched to the round-trip phase in the cavity. Once the laser is operating, control of the MZI phase is sufficient to ensure locking to the main cavity, and there is no need to control the time delay in the MZI. Adjustment of the differential time delay between the MZI arms must only be done during the initial laser startup. As the pulse amplitudes and central frequencies are tightly controlled by the three servo mechanisms during pulsed laser operation, variations in the time delay T_M of the MZI are small and bounded, so that they can in practice be ignored. As always, the time constants characterizing all servo-loops must be much larger than those characterizing the laser dynamics.

In steady-state modelocked operation, the complex envelope of the electric field at a constant arbitrary reference point along the cavity can be written as

$$\sum_k a(t - kT_s)\exp(i\theta_s), \tag{2}$$

where T_s is the repetition period of the pulse train and θ_s is the phase difference between adjacent pulses. The overall round-trip delay and phase slip are therefore NT_s and $N\theta_s$, respectively. In the case of a perfectly matched MZI, when $NT_M = T_R$ and $N\theta_M = \theta_R$, we have $T_s = T_M$ and $\theta_s = \theta_M$, in agreement with our earlier arguments. However, in the more general situation, the waveform $a(t)$, as well as the values of T_s and θ_s depend on the offsets in the MZI time and phase parameters, which we denote by $\Delta T = T_M - T_R/N$ and $\Delta\theta = \theta_M - \theta_R/N$, respectively. It is useful to introduce a special notation for the difference between the MZI parameters and the parameters of the equilibrium pulse-train $\eta_s = T_M - T_s$ and $\phi_s = \theta_M - \theta_s$, which vanish when the MZI is perfectly matched. Using this notation, the signals that go into the input ports of the MZI monitor Δ from the $+120$ and -120 output ports of the 3×3 combiner in Fig. 1 can be expressed in the Fourier domain as

$$\tilde{a}_{\pm}(\omega) \quad = \quad \frac{1}{\sqrt{3}}\left\{\sqrt{1-r^2}] + r\exp\left[i\left(\phi_s + \eta_s\omega \pm 2\pi/3\right)\right]\right\}\tilde{a}(\omega). \tag{3}$$

Consequently, the optical power measured at the two monitor ports, normalized to the overall

#150450 - $15.00 USD Received 5 Jul 2011; revised 26 Aug 2011; accepted 8 Sep 2011; published 1 Nov 2011

power of the lasing signal, is given by

$$\begin{aligned} p_{\pm} &= \frac{1}{2\pi W}\int \mathrm{d}\omega |\tilde{a}_{\pm}(\omega)|^2 \\ &= \frac{1}{3} + \frac{r\sqrt{1-r^2}}{\pi W\sqrt{3}}\int \mathrm{d}\omega \cos\left(\phi_s + \eta_s\omega \pm 2\pi/3\right)|\tilde{a}(\omega)|^2 \\ &\simeq \frac{1}{3} - \frac{2r\sqrt{1-r^2}}{\sqrt{3}}\left[\frac{1}{2} \pm \frac{\sqrt{3}}{2}(\phi_s + \eta_s\langle\omega\rangle)\right], \end{aligned} \tag{4}$$

where $W = \int |a(t)|^2 \mathrm{d}t$ is the energy of an individual pulse, and where

$$\langle\omega\rangle = \frac{1}{2\pi W}\int \mathrm{d}\omega\, \omega |\tilde{a}(\omega)|^2 \tag{5}$$

is the central frequency of the pulse's complex envelope. The last term in (4) is a first-order approximation, valid when the mismatch parameters ϕ_s and η_s are small. Within this same approximation, the feedback control signal is given by

$$m_\theta = p_- - p_+ \simeq 2r\sqrt{1-r^2}\phi_s, \tag{6}$$

where we note that in most cases of interest, the power spectrum of the generated laser pulses is symmetric, implying that $\langle\omega\rangle = 0$. The signal at the third port of the output coupler of the MZI, which is injected back into the laser cavity, can be expressed as

$$\begin{aligned} \tilde{a}_c(\omega) &= \frac{1}{\sqrt{3}}\left\{\sqrt{1-r^2} + r\exp\left[i\left(\phi_s + \eta_s\omega\right)\right]\right\}\tilde{a}(\omega) \\ &\simeq A\left[1 + \rho^2 i(\phi_s + \eta_s\omega) - \frac{1}{2}\rho^2(\phi_s + \eta_s\omega)^2\right]\tilde{a}(\omega), \end{aligned} \tag{7}$$

where we have expanded the exponential, assuming $|\phi_s + \eta_s\omega| \ll 2\pi$, and

$$A = \frac{1}{\sqrt{3}}\left(\sqrt{1-r^2} + r\right), \qquad \rho^2 = \frac{r}{\sqrt{1-r^2} + r}. \tag{8}$$

The factor A represents the intrinsic insertion loss of the MZI, which does not depend on the value of the controlled parameter θ_M. Since this loss may be compensated by amplification in the cavity, its presence is of little importance. The factor ρ can be viewed as the effective coupling coefficient of the MZI, in the sense that the effect of our non-symmetric MZI is equivalent to that of a symmetric MZI that uses identical 2×2 couplers, whose coupling coefficients are equal to ρ. The last form of Eq. (7) suggests that the effect of the MZI is that of modifying the round-trip phase (the term proportional to $i\phi_s$), time delay (the term proportional to $i\eta_s\omega$), chromatic dispersion (the term proportional to ω^2) and attenuation (the term proportional to ϕ^2). In addition, the term proportional to $\phi_s\eta_s\omega$ can be shown to be responsible for a shift in the central frequency of the generated pulses.

3. The steady-state pulses

In order to quantify the effects of the MZI in the proposed set-up, a specific model for signal propagation in the main cavity must be assumed. A convenient choice that illustrates the main features of the MZI enhanced cavity is to assume that in the absence of the MZI the cavity is adequately represented by Haus's master equation model [33]. While this model does not

#150450 - $15.00 USD Received 5 Jul 2011; revised 26 Aug 2011; accepted 8 Sep 2011; published 1 Nov 2011

quantitatively describe any particular laser [34], it captures the key physical issues that must be taken into account, which is sufficient for our purposes. In this model, the contributions of the MZI listed after Eq. (7) can be introduced by simply modifying the master equation parameters. The resultant complex Ginzburg-Landau equation (CGLE) is given by

$$T_R\frac{\partial a}{\partial T}+\Delta t\frac{\partial a}{\partial t} = (g-l')a-\frac{i}{2}(\beta_D+i\beta_g')\frac{\partial^2 a}{\partial t^2}+i(\gamma_K-i\gamma_a)|a|^2a+i\theta_R a, \quad (9)$$

with

$$l' = l+\frac{1}{2}\frac{\rho^2(1-\rho^2)\beta_g\phi_s^2}{\beta_g+\rho^2(1-\rho^2)\eta_s^2}, \quad (10a)$$

$$\beta_g' = \beta_g+\rho^2(1-\rho^2)\eta_s^2, \quad (10b)$$

$$\theta_R' = \theta_R-2\beta_D\left[\frac{\rho^2(1-\rho^2)\eta_s\phi_s}{\beta_g+\rho^2(1-\rho^2)\eta_s^2}\right]^2+\frac{\rho^2\phi_s\beta_g}{\beta_g+\rho^2(1-\rho^2)\eta_s^2}+R\phi_s-R\theta_M, \quad (10c)$$

$$\Delta t = \frac{\beta_D\rho^2(1-\rho^2)\eta_s\phi_s}{\beta_g+\rho^2(1-\rho^2)\eta_s^2}+\rho^2\eta_s. \quad (10d)$$

In Eqs. (9) and (10), the parameters g and l are the per round-trip gain and loss of the main cavity, respectively, β_D is the accumulated dispersion per round-trip, $\beta_g=2g/\Omega_g^2$ accounts for the gain bandwidth limitation (with Ω_g being the bandwidth of the gain spectrum [33],[35]), γ_K is the coefficient of Kerr nonlinearity and γ_a accounts for the effect of saturable absorption. The parameters l', β_g' and θ_R' are modified by the effect of the MZI, and they reduce to their respective unperturbed values l, β_g and θ_R when $\eta_s=\phi_s=0$. Finally, the time offset Δt represents a correction to the the laser round-trip time that is induced by the presence of an imperfectly matched MZI. The central frequency of the signal described by Eq. (9) is assumed to be equal to the peak frequency of the net gain spectrum, which is modified by the frequency dependent loss of the MZI. The MZI-induced shift in the gain peak frequency, is given by

$$\Delta\omega=-\frac{\rho^2(1-\rho^2)\eta_s\phi_s}{\beta_g+\rho^2(1-\rho^2)\eta_s^2}. \quad (11)$$

The values of ϕ_s and of η_s are obtained from imposing self-consistency conditions

$$\theta_R'+\Delta\theta_{\rm NL} = N\theta_s, \quad (12a)$$

$$T_R+\Delta t = NT_s, \quad (12b)$$

which together with the relations $\theta_s=\theta_M-\phi_s$ and $T_s=T_M-\eta_s$, form a set of two algebraic equations from which ϕ_s and η_s can be extracted. When the laser is modelocked, so that Eq. (9) holds, its steady state solutions are chirped hyperbolic secant waveforms, whose parameters can be readily obtained from the coefficients in Eq. (9) [35]. Those coefficients are found from the solution of the self-consistency equations (12), while using the definitions in Eqs. (10). This procedure greatly reduces the computational time that is needed to determine the slow response of the pulses to the combination of the noise and the feedback system.

We next carried out a series of simulations to demonstrate the stability of the multi-pulse solutions. Initially, we demonstrate the accuracy of the approximation that we described in the last paragraph, in which the effect of the MZI on the steady-state solution is to change the pulse parameters, while the pulse waveform still remains a chirped hyperbolic secant. To demonstrate the accuracy of this approximation, we modeled the laser using a CGLE identical to Eq. (9), but with the intrinsic cavity parameters [33, 35], i.e., without using the modifications due to

#150450 - $15.00 USD Received 5 Jul 2011; revised 26 Aug 2011; accepted 8 Sep 2011; published 1 Nov 2011

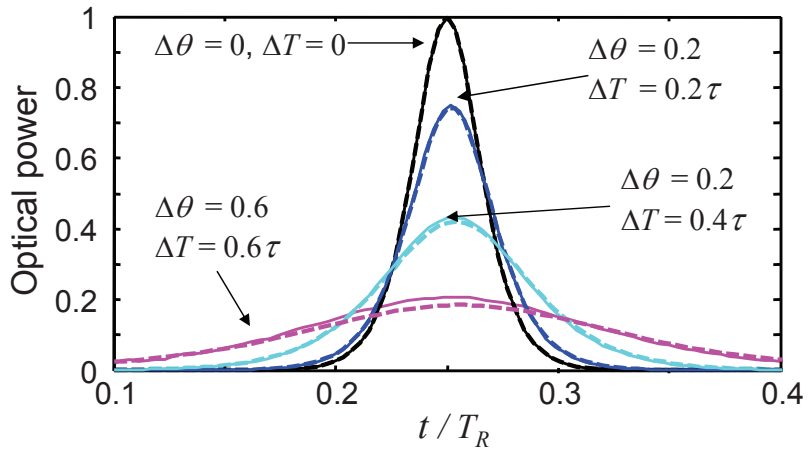

Fig. 2. The steady-state waveform for several values of the MZI time and phase offsets from their ideal values. The solid curves show the computational solution of the full CGLE, while the dashed curves show the approximate solution that we obtain by using a chirped hyperbolic secant waveform with the modified parameters given in Eq. (10). The powers are normalized to the peak power of the steady-state pulse that corresponds to a perfectly-matched MZI.

the MZI that are given by Eq. (10). We solved the CGLE using the split-step Fourier method, and we accounted for the presence of the MZI by imposing appropriate boundary conditions on the computational solution. We also used this computational procedure in order to demonstrate that the multi-pulse laser will start up from noise and converge to a modelocked multi-pulse solution even when the laser parameters are not ideal. Subsequently, we used our approximate steady-state solution, together with a simple first-order model of the feedback system in order to demonstrate that on a longer time scale, the feedback system will drive the laser parameters toward their ideal values.

In order to minimize computation time while elucidating the basic physics, we focused on the case in which there are two pulses in the laser cavity in our studies of the full CGLE. We verified that there are no changes in the basic behavior when the number of pulses is increased to ten. We chose the cavity parameters so that for the case of a perfectly matched MZI, the steady state pulses were classical solitons [35] whose waveform is proportional to $\mathrm{sech}(t/\tau)$ with $\tau = 0.02\,T_R$. We chose the dispersion and nonlinearity coefficients so that the nonlinear and dispersive lengths were both equal to 50 times the length of the cavity. The magnitude of the gain-bandwidth limitation parameter in the CGLE was set equal to -0.5 times the round-trip dispersion coefficient, while the coefficient of saturable absorption was 0.5 times the Kerr coefficient. The average saturation power of the gain medium was taken to be half of the average steady-state power present in the cavity when the MZI matching is perfect. The round-trip loss of the cavity (not including the MZI) was taken to be 0.5 dB, and we set the coupling parameter of the MZI to be $r^2 = 0.5$ in all cases.

Figure 2 compares the steady-state waveform obtained in the simulations with the steady-state waveforms predicted by our theory. The full simulation results are plotted using a solid line, while the steady state-waveforms predicted by the approximate theory are plotted using dashed lines. Deviations between the simulated and approximated waveforms can only be observed when the offset in the parameters is so large that the waveforms are considerably distorted. For proper operation, the actively controlled servo loops should prevent such large

#150450 - $15.00 USD Received 5 Jul 2011; revised 26 Aug 2011; accepted 8 Sep 2011; published 1 Nov 2011

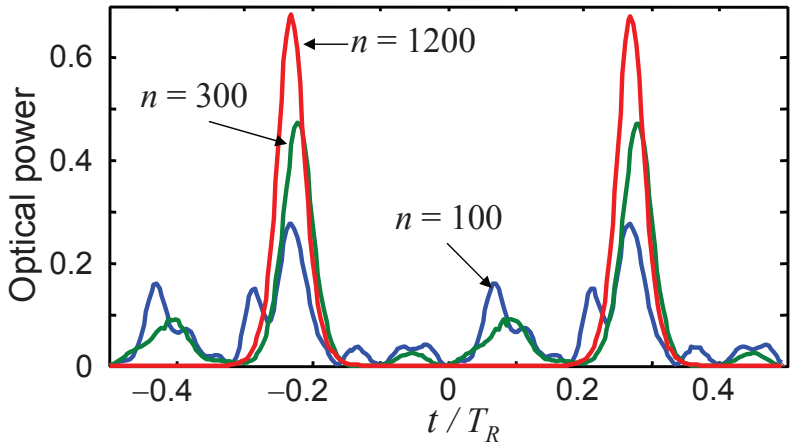

Fig. 3. Buildup of stable pulses from noise. The MZI mismatch parameters are $\Delta T = 0.2\tau$ and $\Delta\theta = 0.3$ rad. The blue, green and red curves correspond to the waveform after 100, 300 and 1200 roundtrips, respectively. The case of $n = 1200$ is indistinguishable from the steady state solution. The powers are normalized to the peak power of the steady-state pulse that corresponds to a perfectly-matched MZI.

offsets at all times. In general, we found that the predictions of our approximate theory are accurate when the phase error of the MZI is smaller than ~ 1 radian and when the timing error is smaller than half the duration of the unperturbed pulse.

In order to illustrate that the laser startup from noise produces stable pulses even when the initial parameters are not ideal, we show in Fig. 3 the evolution of the optical power generated in the cavity for the case in which the phase and time delays of the MZI are offset from perfect matching by $\Delta\theta = 0.3$ radians and $\Delta T = 0.2\tau$, respectively. The generated average noise power is smaller by 40 dB than the average power of the equilibrium pulses under perfect matching conditions. As expected, continuous waves are suppressed, and the pulses grow from noise, as we show in the figure. Convergence occurs in about 1000 round trips, which corresponds to 5 μs in a laser with a round-trip repetition rate of 200 MHz. This time is fast compared to the typical response time of the servo loops. Figure 4 shows a mesh plot of the relation between the time and phase mismatch of the MZI and the amplitude of the MZI feedback parameter m_θ that we introduced in Eq. (6). This curve was obtained by solution of the self-consistency conditions (12). Although the timing mismatch ΔT has some effect on m_θ, this effect is relatively small and m_θ is affected primarily by the phase mismatch $\Delta\theta$.

4. Laser control

The laser parameters that have to be controlled by the servo loops (T_R, θ_R and θ_M) are not identical to the error signals that are produced by the servo loops (ΔT_s, $\Delta\theta_s$ and m_θ), although they are highly correlated. While we could in principle use a linear combination of the error signals to control the laser parameters [36], we will show that it is not necessary. The error signals ΔT_s, $\Delta\theta_s$ and m_θ are so highly correlated to the offset in the laser parameters from their ideal values, ΔT_R, $\Delta\theta_R$ and $\Delta\theta_M$, respectively, that we may use the former to directly control the latter. While the phase-locked loops that control CEPL laser systems are in practice quite sophisticated [37], we will use simple first-order loops, each of which has a response time of 50 μs. When simulating the response of the system to initial perturbations of the laser parameters, we use the approximate steady-state solutions whose accuracy is demonstrated in Fig. 2, and

#150450 - $15.00 USD Received 5 Jul 2011; revised 26 Aug 2011; accepted 8 Sep 2011; published 1 Nov 2011

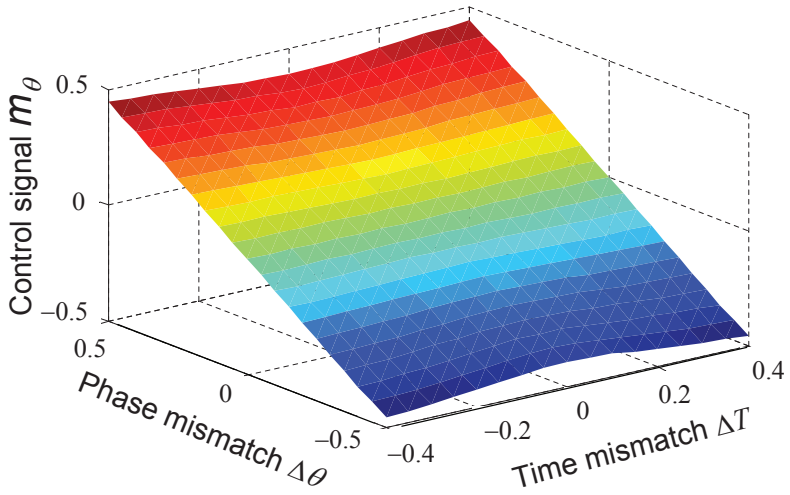

Fig. 4. The value of the monitor signal m_θ as a function of the phase mismatch $\Delta\theta$ and time mismatch ΔT parameters.

which make the simulations computationally tractable.

To demonstrate the stability of this feedback procedure, we show an example of the response of the multi-pulse CEPL laser system to a relatively large initial perturbation of the laser parameters. We consider a laser cavity with a round-trip time $T_R = 5$ ns, corresponding to a round-trip repetition rate of 200 MHz. We set $N = 100$, corresponding to a pulse separation of 50 ps, and we consider a pulse duration of $\tau = 200$ fs. In this example, we set the initial value of ΔT_R to 80 fs, which is a large fraction of the pulse duration. We set the initial values of $\Delta\theta_R$ and $\Delta\theta_M$ to -0.3 and 0.4 radians respectively, which are relatively large perturbations, as we pointed out previously in the context of Fig. 2. We note that although these perturbations are relatively large, they are not so large that the approximations in Eq. (9) become invalid. We show the evolution of the three control signals and the consequent offsets in the laser parameters in Fig. 5, showing that they all approach zero in approximately 200 μs. The high degree of correlation between the control signals and the offsets in the laser parameters is apparent. When we vary the initial offsets of the laser parameters from their ideal values over the parameter range in which Eq. (9) remains valid, we find that the feedback approach that we have proposed remains stable.

5. Discussion and conclusion

To date, while CEPL lasers have revolutionized the measurement of frequencies and time, they are still for the most part laboratory instruments. They are currently too expensive for many applications, and they are often not robust, by which we mean that they require regular intervention by their users. However, the ongoing development of high-power fiber lasers and turnkey CEPL fiber laser systems appears likely to resolve these issues in the near future and enable a host of applications that require plug-and-play laser systems. For many of these applications — particularly RF-photonic applications — it would be desirable to have a 10-GHz repetition rate. It does not appear possible to achieve a fundamental repetition rate in fiber lasers that is above 500 MHz. So, it is necessary to find some way to multiply the fundamental repetition rate. It is possible to do that by using external Fabry-Perot gratings, but this approach divides the per-pulse energy by the square of the multiplication factor. It is more desirable to increase

#150450 - $15.00 USD Received 5 Jul 2011; revised 26 Aug 2011; accepted 8 Sep 2011; published 1 Nov 2011

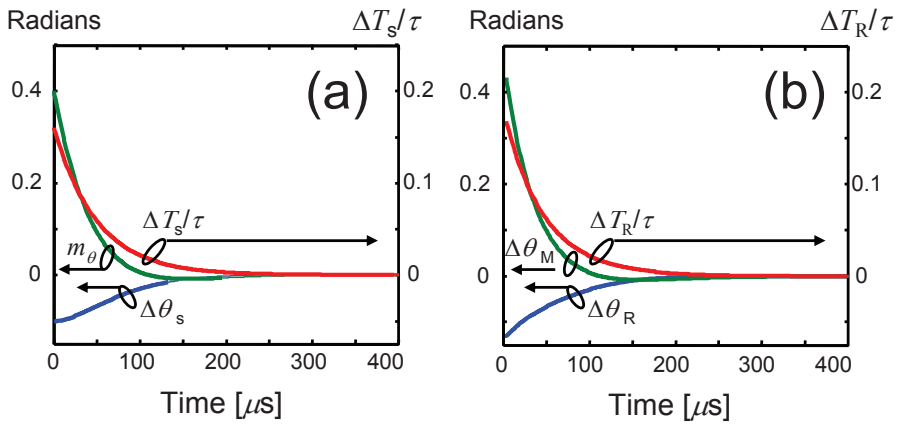

Fig. 5. Evolution of the control signals (a) and the offsets in the laser parameters (b) after a large perturbation. The offsets in the laser parameters ΔT_R, $\Delta\theta_R$, and $\Delta\theta_m$ are highly correlated to the control signals ΔT_s, $\Delta\theta_s$, and m_θ, respectively.

the number of pulses in the laser cavity if the spacing and phase relation between these pulses can be rigidly controlled.

Fiber lasers with multiple pulses are easy to obtain [21]. As pump powers increase, it is common for a single pulse in a laser cavity to break up into multiple pulses. However, the pulses will naturally drift about and collide with each other due to noise or other perturbations. In actively modelocked lasers, the modelocking mechanism locks the pulse spacing, and it is possible to have many pulses in the cavity at once with a fixed spacing. However, the pulses are not short enough to achieve carrier-envelope phase-locking. Because the round-trip phase is unlocked, it can slip, leading to supermodes. In passively modelocked lasers, it has not been possible to rigidly lock the pulse spacing in multi-pulse lasers. In this paper, we present an approach that can solve this problem.

The key barrier to locking the pulse spacing has been the lack of a robust feedback mechanism that can fix the spacing and the phase relation. An ideal feedback signal should pass through zero at the optimal operating point with a large derivative. The 3×3 coupler that we are proposing produces this result. To be realizable in practice, multi-pulse solutions must arise from noise even when the laser parameters are not ideal, and the feedback system must force the laser systems towards its ideal parameter values even when the parameters are far from ideal. To demonstrate the first point, we solved the laser model computationally. The second point has been demonstrated with the help of a reduced model that we developed for this purpose and whose accuracy has been validated by comparison with numerical solutions.

In conclusion, we have presented a scheme for using an intra-cavity Mach-Zehnder interferometer, with appropriate monitor signals, to stably lock multiple pulses inside a fiber laser cavity. This approach builds on well-established carrier-envelope phase-locking technology by adding one more phase-locked loop to the system. In contrast to approaches that use external Fabry-Perot cavities to essentially filter out unwanted tones in the frequency comb, the approach presented here will in principle enhance the power output of the laser by a factor N and the power in each of the lines by a factor N^2, where N is the number of pulses in the cavity. We have demonstrated the stability of this approach for a multi-pulse cavity by showing that a laser with large perturbations will relax back to its ideal parameter set and by showing that multiple pulses can start up from noise even when the initial parameter set is not ideal.

#150450 - $15.00 USD Received 5 Jul 2011; revised 26 Aug 2011; accepted 8 Sep 2011; published 1 Nov 2011

Acknowledgements
The authors gratefully acknowledge useful discussions with T. F. Carruthers and A. Mecozzi. Work at UMBC was supported in part by the Johns Hopkins University Applied Physics Laboratory.

#150450 - $15.00 USD Received 5 Jul 2011; revised 26 Aug 2011; accepted 8 Sep 2011; published 1 Nov 2011